Loss of *ZNF251* stimulates NHEJ resulting in PARP inhibitor resistance in *BRCA1*-mutated cancer cells

Huan Li[1], Srinivas Chatla[2], Xiaolei Liu[3], Matthew Walt[1], Dongwook Kim[1], Zhaorui Lian[1], George Morton[4], Zijie Feng[5], Dan Yang[1], Hongjun Liu[6], Katherine Sullivan-Reed[2], Wayne Childers[4], Xiang Yu[7], Jozef Madzo[1], Kumaraswamy Naidu Chitrala[2], Tomasz Skorski[2,*], Jian Huang[1,8,9,*]

[1]Coriell Institute for Medical Research, Camden, NJ, United States

[2]Temple University Lewis Katz School of Medicine, Fels Cancer Institute for Personalized Medicine and Department of Cancer and Cellular Biology, Philadelphia, PA, United States

[3]Department of Medicine, Perelman School of Medicine at the University of Pennsylvania, Philadelphia, PA, United States

[4]Moulder Center for Drug Discovery Research, School of Pharmacy, Department of Pharmaceutical Sciences, Temple University, Philadelphia, PA, United States

[5]Department of Cancer Biology, Abramson Family Cancer Research Institute, Institute of Diabetes, Obesity, and Metabolism, University of Pennsylvania Perelman School of Medicine, Philadelphia, PA, United States

[6]IPhase Pharma Services LLC, Beijing, PR China

[7]Shanghai Jiao Tong University, School of life Science and Biotechnology, Shanghai, PR China

[8]Temple University Lewis Katz School of Medicine, Center for Metabolic Disease Research, Philadelphia, PA, United States

[9]Cooper Medical School of Rowan University, Camden, NJ, United States

*Correspondence: Jian Huang, jhuang@coriell.org; Tomasz Skorski, tomasz.skorski@temple.edu

Running title: ZNF251 for PARPis resistance

Abstract

The poly (ADP-ribose) polymerases (PARPs) inhibitors are an exciting new class of agents that have shown efficacy in treating various cancers, especially those harboring *BRCA1/2* mutations. The cancer associated *BRCA1/2* mutations disrupt DNA double strand break (DSB) repair by homologous recombination (HR). PARP inhibitors (PARPi) have been applied to trigger synthetic lethality in *BRCA1/2*-mutated cancer cells by promoting the accumulation of toxic DSBs. Unfortunately, PARPi resistance is common and develops through multiple mechanisms. Restoring HR and/or stabilizing replication forks are two major mechanisms of PARPi resistance in *BRCA1/2*-mutated cells. To further understand the mechanisms of drug resistance to PARPi, we took an unbiased approach with a CRISPR-pooled genome-wide library to screen new genes whose loss-of-function confers resistance to PARPi olaparib. We identified ZNF251, a transcription factor, and found that its loss-of-function led to the PARPi resistance in multiple *BRCA1*-mutated breast and ovarian cancer lines. Elevated activities of both HR and non-homologous end joining (NHEJ) repair were detected in cancer cells harboring *BRCA1* mutation and *ZNF251* deletion (*BRCA1*mut+*ZNF251*del) and were associated with enhanced expression of RAD51 and Ku70/Ku80, respectively. Furthermore, we showed that a DNA-PKcs inhibitor restored sensitivity of *BRCA1*mut+*ZNF251*del cells to PARPi *ex vivo* and *in vivo*. Taken together, our study discovered a novel gene *ZNF251* whose loss-of-function conferred resistance to PARPi in *BRCA1*-mutated breast and ovarian cancers and identified DNA repair pathway responsible for this effect.

Introduction

The poly (ADP-ribose) polymerases (PARPs) — also known as NAD+ ADP-ribosyltransferases — are an emerging family of 18 enzymes that share the ability to catalyze the transfer of ADP-ribose to target proteins (poly ADPribosylation)(1,2). PARPs play an important role in various cellular processes, including modulation of chromatin structure, transcription, replication, recombination, and DNA repair(3). PARP1 is the most potent enzyme of this group and accounts for 80–90% of DNA damage-induced PARylation; it also plays a key role in DNA damage response (DDR), including the repair of DNA single-strand breaks (SSBs) and double-strand breaks (DSBs)(4-6). SSBs are repaired by PARP1-mediated base-excision repair (BER). DSBs may be repaired by three classical pathways: BRCA1/2-dependent homologous recombination (HR), DNA-PKcs-mediated nonhomologous end joining (NHEJ), and PARP1-

mediated alternative NHEJ (Alt-NHEJ). These DNA repair pathways can either work independently or coordinately to prevent/repair different types of DSBs.

Mutations in the *BRCA1/2* genes that result in dysfunctional HR incur a high risk of breast and ovarian cancer development. Both BRCA1 and BRCA2 interact with various proteins involved in the HR repair pathway and appear indispensable for this process, acting at different stages in DSB repair. Because PARPi induce DSBs that are dependent on the HR pathway for repair, cells with dysfunctional HR due to BRCA1/2 mutations are particularly sensitive to the treatments with PARPi(3,7). Current FDA-approved PARP1 inhibitors (PARPis: olaparib, rucaparib, niraparib, talazoparib) are NAD+ competitors, thus blocking the poly (ADP ribose) polymerase activity. Failure to repair SSB lesions due to PARP1 inhibition generates toxic DSBs in cells displaying HR deficiency, resulting in synthetic lethality. Unfortunately, the majority of patients with *BRCA1/2* mutated tumors who initially show improvements after PARPi treatment develop resistance to PARP inhibitors, which results in disease progression. To explore the novel molecular mechanisms of PARPi resistance, we performed a genome wide CRISPR screen for gene mutations that confer resistance to the PARP inhibitor olaparib.

Here, we report that deletion mutations in zinc finger 251 (*ZNF251* KO) cause resistance to olaparib in multiple *BRCA1*-mutated cancer cells. Furthermore, *BRCA1*-mutated *ZNF251* KO (*BRCA1*mut+*ZNF251* KO) breast cancer cells were resistant not only to various PARPi, but also to platinum-based drugs and DNA polymerase θ (Polθ) inhibitors. Mechanistically, we found that activation of the DNA-PKcs-mediated NHEJ repair pathway was the major mechanism of olaparib resistance conferred by *ZNF251* KO in *BRCA1*-mutated cells. Importantly, we further demonstrated that a DNA-PKcs inhibitor restored sensitivity of *BRCA1*mut+*ZNF251* KO breast cancer cells to PARPi *ex vivo* and *in vivo*.

Materials and Methods

Cell lines and cell culture

MDA-MB-436 and HCC1937 were purchased from ATCC. MDA-MB-436 and Ovcar8 cells were maintained in DMEM supplemented with 10% FBS and 1% penicillin/streptomycin. HCC1937 cells were cultured in RPMI 1640 supplemented 10% FBS and 1% penicillin/streptomycin. All cell lines were analyzed and authenticated by morphologic inspection and biochemical examination of the *BRCA1* mutation pathway as well as short tandem repeat profiling analysis.

Mycoplasma testing was also performed to exclude the possibility of mycoplasma contamination of all cell lines.

Chemical Compounds

Olaparib (Catalog# A4154), cisplatin (Catalog# A8321), carboplatin (Catalog# A2171), and 5-fluorouracil (Catalog# A4071) were all purchased from APExBIO company. UPF 1096 (Catalog# S8038), NMS-P118(Catalog# S8363), stenoparib (E7449) (Catalog# S8419), niraparib (Catalog# S2741), rucaparib (Catalog# S4948), and veliparib (ABT-888) (Catalog# S1004) were all purchased from Selleckchem. Cisplatin (Catalog# A10221) was purchased from AdooQ Bioscience. ART-558(Catalog# HY-141520), DNA-PK inhibitor PIK-75 hydrochloride (Catalog# HY-13281), RAD51 Inhibitor B02 (Catalog# HY-101462), and olaparib (for *in vivo* experiment: Catalog# HY-10162) were all purchased from MCE (MedChem Express). ART-812 was synthetized by Dr. Wayne Childers at Temple University School of Pharmacy. All compounds were dissolved, aliquoted, and stored following the manufacturer's instructions.

Pooled Genome-Wide CRISPR/Cas9 Screen

The GeCKO CRISPR library was purchased from Addgene (#1000000048), amplified, and packaged as lentivirus based on the instructions on Addgene website. The CRISPR screen was performed as described previously(8). In brief, MDA-MB-436 cells were transduced with lentivirus carrying GeCKO library, and puromycin selection was performed for 3 days. Then we treated transduced MDA-MB-436 cells with olaparib for 14 days, the medium was changed with adding fresh olaparib every three days during 14 days screen, and the surviving cells were harvested. The genomic DNA was extracted, and PCR was carried out before deep sequencing of sgRNA sequence in the surviving cells' genome. All deep sequencing data are available at GEO (series accession number GSE205221). For data analysis, we calculated the enrichment score as: The enrichment score= (sgRNA number from the reads)/ (sgRNA number in the library) X $\log_2$ (average abundance). The sgRNAs used for validations were synthesized and constructed as described(8). Primer sequences are shown in Supplementary Table S1.

T7EN1 assays and DNA sequencing

The T7EN1 assay was performed as described previously(8). To identify the *ZNF251* mutations, the PCR product was sequenced by Sanger sequencing. The primers used for Sanger sequencing were listed in Supplementary Table S1.

Generation of mutant single clones

500 transduced MDA-MB-436 cells were mixed with 1 ml of methylcellulose (MethoCult H4034 Optimum, Stem Cell Technologies) in a 6-well cell culture plate and cultured at 37 °C in a 5% CO_2 incubator. Two weeks later, single colonies were picked and cultured in a 96-well plate with the complete medium supplemented with 2% penicillin/ streptomycin. The cells were passaged every two or three days, and 1/3 of cells were collected for genomic DNA extraction. Then *ZNF251* target region was PCR amplified and sequenced.

Cell viability assay

1×10^4 cells were cultured with 100μl of complete medium in a 96-well plate and treated as indicated. Cell viability was measured at different time points as described with the trypan blue exclusion viability test. The final viable cell number was calculated based on the growth standard curve. All the key viability experiments were confirmed by the MTS assay (Promega, Catalog# G3582) and CCK-8 assay (APExBIO company, Catalog# K1018).

Off-target effect examination

Off-target sites were predicted using an online search tool (http://crispr.mit.edu). 3bp mismatches compared with the target consensus sequence were allowed. The predicted off-target sequences were searched using UCSC browse, and 500bp flanking the sites were PCR-amplified in primary cells and single mutation clones. The PCR product was subjected to the T7EN1 assay to determine the mutation. The PCR product was then cloned into a TA vector and Sanger sequenced to identify mutations.

Immunoblot analysis

Nuclear and total cell lysates were obtained as described before(9) and analyzed by SDS-PAGE using primary antibodies against: ATM (Santa Cruz Biotechnology #sc-135663), CtIP (Abcam #ab-70163), 53BP1 (Abcam #ab-175933), SLFN11 (Santa Cruz Biotechnology #sc-515071), BRCA1 (ThermoFisher Scientific #MA1-23164), BRCA2 (Santa Cruz Biotechnology #sc-28235), PALB2 (Proteintech #14340-1-AP), RAD51 (Abcam #ab-88572), RAD52 (Santa Cruz Biotechnology #sc-365341), RAD54 (Santa Cruz Biotechnology #sc-374598), DNA-PKcs (Bethyl #A300–518A), Ku70 (Santa Cruz Biotechnology #sc-17789), Ku80 (ThermoFisher Scientific #MA5–15873), DNA ligase 4 (ThermoFisher Scientific #PA5-40826), PARP1 (Santa Cruz Biotechnology #sc-74470), PARP2 (Santa Cruz Biotechnology #sc-393310), PARP3 (Santa Cruz Biotechnology #sc-390771), DNA ligase 3 (Santa Cruz Biotechnology #sc-135883),

Polθ (MyBioSource #MBS9612322), lamin B (Abcam #ab-16048–100), and β-actin (Santa Cruz Biotechnology #sc-47778) and the following secondary antibodies conjugated to HRP (horseradish peroxidase): goat anti-rabbit (EMD Millipore #12–348) and goat anti-mouse (EMD Millipore #AP181P). For quantification of western analysis, ImageJ software was used to measure the density of the protein bands.

DNA damage/repair assays

DSBs were detected by neutral comet assay as described before(9) with modifications. Briefly, comet assays were performed using the Oxiselect Comet Assay Kit (Cell Biolabs #STA-355) according to the manufacturer's instructions. Images were acquired by an inverted Olympus IX70 fluorescence microscope using a FITC filter, and the percentage of tail DNA of individual cells was calculated using the OpenComet plugin of ImageJ. HR, D-NHEJ, and Alt-NHEJ were measured using DR-GFP (HR), EJ2-GFP (D-NHEJ), and EJ5-GFP (Alt-NHEJ) reporter cassettes as described before(9). Briefly, the reporter plasmid was digested by I-SceI endonuclease, and the repaired GFP cells were counted by flow cytometer. The result was calculated by total restored GFP positive cells / total transfected M-cherry or BFP positive cells.

Mice and *in vivo* studies

6-8 weeks-old female NOD/SCID/IL-2Rγ (NSG) mice (Jackson Laboratories) were injected subcutaneously with $1x10^6$ MBA-MD-436 cells in the flank. Mice were randomized to treatment groups when tumor sizes reached 50-60 mm^3. For the first set of the experiments, all animals with wildtype or *ZNF251* KO tumors of 50-60 mm^3 were randomized into two groups (n=4/group), which were intraperitoneally treated with vehicle or olaparib (10mg/kg) daily for four weeks, respectively. For the second set of experiments, all mice were randomly divided into four groups and intraperitoneally injected daily with either vehicle, olaparib (10mg/kg), DNA-PK inhibitor PIK-75 (10mg/kg), or olaparib (10mg/kg) plus PIK-75(10mg/kg) for four weeks. Since the start of the experiment, tumor volumes (V) were measured every three days based on the formula $V = L \times W^2 \times 0.5$, where L represents the largest tumor diameter and W represents the perpendicular tumor diameter(10). After four weeks, all mice were euthanized and tumors were dissected out, imaged, weighed, or used for further characterization. All experiments involving animals were approved by the Cooper University and the IPhase Pharma Services LLC Institutional Animal Care and Use (IACUC) Committee.

Bioinformatics analysis of *ZNF251* expression in the cells sensitive and resistant to PARPi olaparib

To analyze the expression of *ZNF251* expression in the cells sensitive and resistant to PARPi olaparib, we performed bioinformatics analysis. Datasets for the respective inhibitors were downloaded from the Gene Expression Omnibus database (http://www.ncbi.nlm.nih.gov/geo), a large public repository for high-throughput molecular abundance data — specifically, gene expression data(11). Dataset GSE165914 was utilized for the analysis of *ZNF251* expression in olaparib sensitive and resistant cells(12). Statistical analysis was performed using the Graph Pad Prism 9.

Quantification and Statistical Analysis

All statistical analyses were performed by GraphPad Prism 8. Cell viability data were analyzed by two-way ANOVA tests. The neural comet assay data was analyzed by Mann-Whitney Rank Sum Test. The data of DNA repair assay and *in vivo* experiments were analyzed by unpaired t-test with Welch's correction.

Results

Loss-of-function CRISPR screen identified ZNF251 as a critical factor regulating sensitivity of BRCA1-mutated cells to PARPis

To identify genes whose loss-of-function confers drug resistance to the PARPi olaparib, we performed a genome-wide CRISPR genetic screen in MDA-MB-436 cells, a human breast cancer line harboring a *BRCA1* mutation and which is sensitive to PARPi(13). We used GeCKO CRISPR library which has been demonstrated to be a very efficient tool to screen for mutations that confer resistance to a BRAF inhibitor in a melanoma line(14). First, we packed the library into lentivirus with optimal titer at a multiplicity of infection (MOI) of 0.3-0.4 and transduced MDA-MB-436 cells. After viral transduction, we treated the MDA-MB-436 breast cancer cells with either 0.3 μM or 1μM olaparib, an optimal dose chosen based on our preliminary tests (Supplementary Fig. 1A, B). After 14 days of treatment, we harvested living cells from the olaparib-treated group and extracted genomic DNA for PCR the region containing sgRNAs. Then, we conducted next-generation sequencing (deep sequencing) to identify sgRNAs enriched in olaparib-resistant cells (Fig. 1A). For several genes, we found enrichment of multiple sgRNAs, suggesting that loss of these genes contributes to olaparib resistance (Fig. 1B, C).

Then, we ranked the positive hits by the number of the sgRNAs and enrichment changes per sgRNA. Interestingly, we identified several zinc finger genes as our highest-ranking genes in our screen. *ZNF251* was one of our top hits whose loss-of-function caused resistance to both 0.3 μM and 1 μM of olaparib in *BRCA1*-mutated breast cancer cells.

To validate whether deletion of *ZNF251* confers resistance to olaparib, we used three newly designed sgRNAs to knock out *ZNF251* in the MDA-MB-436 breast cancer cell line. We transduced cells with lentivirus-carrying sgRNAs specifically for *ZNF251* and performed the T7 Endonuclease I assay five days after transduction to determine the knockout efficiency. We found that the efficiency of gene disruption ranged from 52.3% to 89% for all sgRNAs tested (Fig. 1D, top panel). Next, we used these cells to test whether deletion of *ZNF251* can confer resistance to olaparib. Consistent with our screening data, we found that *ZNF251* knockout cells showed marked resistance to treatment with olaparib compared with the parental cells (Fig. 1D bottom panel). Because the CRISPR/Cas9 genome editing system can create a spectrum of insertions/deletions (in/dels) in a cell population, we also isolated three *ZNF251* knockout single clones, sequenced each clone, and found in/dels in all three *ZNF251* knockout clones (Fig. 1E top panel). Next, we tested drug resistance of three independent *ZNF251*-mutated clones to olaparib. Consistent with the data from the heterogeneous population of CRISPR-mutated cells, all three *ZNF251* mutated clones showed strong resistance to olaparib compared with the parental cells (Fig. 1E bottom panel). The IC_{50} of *ZNF251*-deleted clones to olaparib was between 7.04 and16.03 μM, whereas the IC_{50} for parental cells was 4.36 μM. Of note, we transfected *ZNF251* knockout cells with wildtype *ZNF251* cDNA on an ectopic expression plasmid, and it dramatically reversed resistance to olaparib, indicating that it was *ZNF251* deficiency caused this resistance (Supplementary Fig. 2).

To address the question of whether the resistance is correlated with *BRCA1* mutation, we knocked out *ZNF251* in an isogenic *BRCA1*-wildtype and -mutated HCC1937 human breast cancer cell lines. We found that *ZNF251* knockout caused olaparib resistance in *BRCA1*-mutated but not *BRCA1*-wildtype breast cancer cells (Fig. 1F). We subsequently assessed whether *ZNF251* KO caused PARPi resistance *in vivo*. Experimentally, we tested the effect of olaparib on the growth of parental (*ZNF251* wildtype) and *ZNF251* KO MDA-MB-436 cell xenografts in immune-deficient NSG mice. First, we injected either $1x10^6$ wildtype or *ZNF251* KO cells subcutaneously into the flank of 16 NSG female mice (a randomized 8 and 8 mice with either wildtype or *ZNF251* KO cells). Of note, tumors were observed in all 16 animals

transplanted with MDA-MB-436 cells in ~3-4 weeks. Next, all animals carrying wildtype or *ZNF251* KO tumors of 50-60 mm^3 were randomized into two groups (n=4/group), which were intraperitoneally treated with vehicle or olaparib (10mg/kg) daily for four weeks. Consistent with the resistant phenotype, we observed that the tumor size and weight of the olaparib-treated *ZNF251* KO group was significantly bigger than the wildtype group (Fig. 1G, H). At the same time, there were no statistically significant differences between wildtype and *ZNF251* KO tumors in vehicle-treated mice. This shows that *ZNF251* KO breast cancer cells were resistant to olaparib treatment *in vivo*.

Knockout of ZNF 251 confers resistance to multiple PARPis in BRCA1-mutated cells

To test whether deletion of *ZNF251* in breast cancer cells induces resistance to additional PARPis, we tested the resistance of *ZNF251* knockout in MDA-MB-436 cells to several potent PARPis, including niraparib (PARP1/2 inhibitor), veliparib (PARP1/2 inhibitor), NMS-P118 (selective PARP1 inhibitor), and stenoparib (PARP1/2 and PARP5a/5b inhibitor). Consistently, we observed that *ZNF251* knockout breast cancer cells were resistant to all those PARPis (Fig. 2A). To confirm our finding in a *BRCA1*-mutated ovarian cancer line, we knocked out *ZNF251* in the Ovcar8 cell line, a human ovarian cancer line with *BRCA1* mutation, and tested their response to multiple PARPis. We found that *ZNF251*-deleted ovarian cancer cells were also resistant to those PARPis compared with the *ZNF251*-wild type cells (Fig. 2B and data not shown for NMS-P118). Importantly, in the absence of drug treatment, the growth rate of *ZNF251*-null breast and ovarian cancer cells was indistinguishable from their wildtype parental cells (Supplementary Fig. 3). To collect more evidence to support our finding, we also performed bioinformatic analysis of previously published PARPi resistance studies and found significantly lower expression of *ZNF251* in two olaparib-resistant breast cancer cell lines (MDA-MB-468 and SUM1315 lines) when compared to their sensitive counterparts (Supplementary Fig. 4A)(11,12), showing that low expression of *ZNF251* is correlated with olaparib resistance. Furthermore, using CellMiner database analysis, we found that *ZNF251* expression is also positively correlated with sensitivity to olaparib, cisplatin, and carboplatin in breast cancer cells (Supplementary Fig. 4B-D). Consistently, low *ZNF251* expression is correlated with worse survival for breast cancer patients as shown using the online Kaplan-Meier plotter (https://kmplot.com/analysis/index.php?p=service&cancer=breast), which integrates gene expression and clinical data from 2,032 patients(15) (Supplementary Fig. 4E).

Taken together, *ZNF251* deletion in both breast and ovarian *BRCA1*-mutated cancer cells leads to drug resistance to multiple PARPis.

Knockout of ZNF 251 confers resistance to platinum-based drugs in BRCA1-mutated cells

Platinum-based anticancer drugs — including cisplatin, carboplatin, oxaliplatin, nedaplatin, and lobaplatin — are also commonly used first-line chemotherapy regimens in cancer treatment. Mechanistically, these drugs form highly reactive platinum complexes that bind and crosslink DNA in the cancer cells. The mechanisms of action of platinum-based drug and PARP are complementary in many ways and critically reliant on the intracellular DNA damage(16). It was reported previously that resistance to PARPis also resulted in platinum-based drug resistance(17,18). Therefore, we tested whether *ZNF251* KO breast cancer cells were resistant to platinum-based drugs. Experimentally, we treated *ZNF251* KO MDA-MB-436 cells with two platinum-based drugs — cisplatin and carboplatin, respectively — and tested drug resistance. As we expected, *ZNF251* KO MDA-MB-436 cells were resistant to both cisplatin and carboplatin (Fig. 3A, B). The IC_{50} of *ZNF251*-deleted breast cancer cells to cisplatin was 12.54-22.35 μM, whereas the IC_{50} for control cells was 1.93 μM. This indicates that knockout of *ZNF251* confers resistance to platinum-based drugs in *BRCA1*-mutated breast cancer cells. Intriguingly, *ZNF251* KO breast cancer cells were not resistant to 5-fluorouracil (5-Fu), which is primarily a thymidylate synthase (TS) inhibitor (Fig. 3C).

Knockout of ZNF 251 confers resistance to DNA polymerase theta (Polθ) inhibitors in BRCA1-mutated cells

Recent studies have suggested that HR-deficient cancer cells are sensitive to Polθ inhibitors due to synthetic lethality(19,20). Moreover, HR-deficient cells resistant to PARPi could be sensitive to DNA Polθ inhibitors (19,20). To test whether *BRCA1*-mutated *ZNF251* KO breast cancer cells are sensitive to DNA Polθ inhibitors, we treated MDA-MB-436 WT and *ZNF251* KO cells with Polθ DNA polymerase inhibitors ART-558 and ART-812(20) followed by the clonogenic assay. Interestingly, *ZNF251* KO cells showed resistance to Polθ inhibitors (Fig. 4A, B). These results suggest that the deletion of the *ZNF251* gene confers the resistance to Polθ and PARP inhibitors in HR-deficient MDA-MB-436 cells.

ZNF251 KO increases HR and NHEJ repair with treatment of olaparib

To determine the molecular mechanisms by which *ZNF251* deletion confers drug resistance to PARPi, we first examined DSBs by neutral comet assay in *BRCA1*-mutated wildtype and *ZNF251* KO MDA-MB-436 cells treated with olaparib. We found that *ZNF251* KO MDA-MB-436 cells accumulated less olaparib-induced DSBs when compared to wildtype counterparts and were similar to those detected in *BRCA1*-restored cells (Fig. 5A), which suggests a restoration of DSB repair in *ZNF251* KO cells. Therefore, we next examined whether *ZNF251* KO affects DSB repair. Three specific reporter cassettes measuring homologous recombination (HR), non-homologous end joining (D-NHEJ), and alternative non-homologous end joining (Alt-NHEJ) repair activities were applied as described before(9). Interestingly, we found that NHEJ was already markedly upregulated in *ZNF251* KO MDA-MB-436 and Ovcar8 cells before the treatment of olaparib. After the olaparib treatment, both HR and NHEJ responses in MDA-MB-436 and Ovcar8 cells were dramatically upregulated in *ZNF251* KO compared to the wildtype control (Fig. 5B), which suggests that upregulation of both repair pathways contributed to the PARPi resistance of breast and ovarian cancer cells.

To evaluate specific alterations in DSB repair pathways induced by *ZNF251* KO, we also performed western blot analysis to examine the expression of key components of HR, NHEJ, and Alt-NHEJ. We found that Ku70 and Ku80 — which are the key components of the canonical DNA-PKcs-dependent NHEJ pathway (D-NHEJ) — were upregulated in *ZNF251* KO cells treated or not with olaparib (Fig. 5C, Supplementary Fig. 5C). This observation supports the enhanced D-NHEJ activity detected in untreated and olaparib-treated *ZNF251* KO cells. Furthermore, we observed an increased expression of BRCA2 and RAD51 — the key elements of the HR pathway in olaparib-treated *ZNF251* KO MDA-MB-436 cells (Fig. 5C, Supplementary Fig.5B) — consistent with stimulation of HR in olaparib-treated *ZNF251* KO cells (Fig. 5B). The lack of BRCA1 is most likely compensated by overexpression of CtIP in olaparib-treated cells(21). Our RNA-seq analysis revealed that enhanced expression of these genes was not detected in *ZNF251* KO cells (Supplementary Table S2). Altogether, these findings clearly suggest that *ZNF251* KO cells may employ D-NHEJ and/or HR to repair olaparib-triggered DSBs to confer the PARPi resistance.

BRCA1-mutated ZNF251 KO cells are sensitive to DNA-PKcs inhibitor

Reactivation of HR pathway was reported before to cause resistance to PARPis(17). Intriguingly, treating *ZNF251* KO MDA-MB-436 cancer cells with RAD51 inhibitor B02 did not reverse the olaparib resistance (Fig. 6A and Supplementary Fig.6). Thus, stimulation of HR

pathway in olaparib-treated *ZNF251* KO *BRCA1*-mutated breast cancer cells might not play a key role in this resistance. To test if constitutively enhanced activity of the D-NHEJ pathway in *ZNF251* KO contributes to the PARPi resistance, we treated *ZNF251* KO MDA-MB-436 cells with olaparib and/or PIK-75, a DNA-PKcs inhibitor. Remarkably, we found that PIK-75 treatment reversed olaparib resistance of *ZNF251* KO MDA-MB-436 cells (Fig. 6B), indicating that stimulation of D-NHEJ in *ZNF251* KO cells significantly contributed to the olaparib resistance.

To test whether a blockade of the D-NHEJ pathway reversed PARPi resistance of *ZNF251* KO in *vivo*, we treated tumor-bearing mice with olaparib and PIK-75 in combination and compared to olaparib or PIK-75 monotherapy. Experimentally, $1x10^6$ olaparib-resistant *ZNF251* KO MDA-MB-436 cells and olaparib-sensitive *ZNF251* wildtype MDA-MB-436 cells were bilaterally implanted subcutaneously to the right and left flank of each NSG mouse, respectively (Fig. 6C). Of note, tumors were observed in all 20 animals transplanted with wildtype and *ZNF251* KO MDA-MB-436 in ~3-4 weeks. Next, all animals with tumors of 50-60 mm^3 were randomized into four groups (n=5/group), which were intraperitoneally treated with vehicle, olaparib (10mg/kg), PIK-75 (10mg/kg), or olaparib and PIK-75 in combination. Tumor volume and tumor weight were measured at 28 days post-treatment. As expected, olaparib treatment diminished *ZNF251* wildtype MDA-MB-436 tumor volume and weight by 81% and 77%, while *ZNF251* KO MDA-MB-436 tumors were completely resistant (Fig. 6D, E). Remarkably, PIK-75 applied in combination with olaparib reduced *ZNF251* KO MDA-MB-436 tumor volume and weight by 72% and 60%. This clearly demonstrates that blockade of D-NHEJ pathway abrogates the growth of PARPi-resistant *ZNF251* KO MDA-MB-436 breast cancer cells *in vivo*.

Discussion

Four main mechanisms of PARPi resistance have been identified so far in BRCA1/2-mutated cancer cells: alteration of drug availability, modulation of de-PARylation enzymes, restoration of HR, and enhanced replication fork stability(7,22). Using the positive whole-genome CRISPR/Cas9 library screen, we discovered that *ZNF251* deletion caused resistance to PARP inhibitors in *BRCA1*-mutated cancer cells. Our finding is confirmed with multiple *BRCA1*-mutated breast and ovarian cancer lines and PARP inhibitors. *ZNF251* knockout triggered unique mechanisms of PARPi resistance relying on constitutive stimulation of D-NHEJ. Although we cannot completely rule out the contribution of HR pathway activation to *ZNF251* KO-caused PARPi resistance, the RAD51 inhibitor treatment did not reverse the resistance suggested that it didn't play a critical role in this setting. According to our knowledge, stimulation of D-NHEJ was not reported before as a sole mechanism of resistance to PARP inhibitors.

Importantly, *BRCA1*mut+*ZNF251* KO cells were sensitive to a DNA-PKcs inhibitor *in vitro* and *in vivo*, suggesting possible a novel therapeutic solution.

ZNF251 belongs to the Kruppel-associated box (KRAB) zinc-finger gene family cluster and contains the KRAB transcriptional repressor domain. Interestingly, we found that elevated level of Ku70 and Ku80 in *ZNF251* KO cells was not associated with elevated levels of specific mRNAs. Therefore, constitutive overexpression of Ku70 and Ku80 resulting in activation of D-NHEJ in *BRCA1mut ZNF251* KO cells might depend on transcriptional activation associated with the loss of KRAB repressor activity on the genes involved in regulating translation and/or protein degradation of Ku70 and Ku80.

ZNFs have been reported to regulate DNA damage response, including DSB repair(23,24). This is in concordance with reports that ZNFs were capable to stimulate (E4F1, ZNF506, ZNF384) and repress (ZNF280C) DSB repair mechanisms such as D-NHEJ and HR(24-27). Thus, alterations in ZNFs expression may represent a novel diagnostic tool to pre-screen patients with *BRCA1/2*-mutated tumors for potential treatment with PARP inhibitors. The detailed molecular mechanism of ZNFs' function in PARPi resistance still warrants further investigation.

Disclosure of Potential Conflicts of Interest

No potential conflicts of interest were disclosed by any of the authors.

Authors' Contributions

Conception and design: T. Skorski, J. Huang

Development of methodology: H. Li, Z. Lian, T. Skorski, J. Huang

Acquisition of data (provided animals, acquired and managed patients, provided facilities, etc.): H. Li, S. Chatla, X. Liu, D. Kim, Z. Lian, D. Yang, H. Liu

Analysis and interpretation of data (e.g., statistical analysis, biostatistics, computational analysis): H. Li, S. Chatla, M. Walt, Z. Lian, X. Yu, J. Madzo

Writing, review, and/or revision of the manuscript: H. Li, S. Chatla, J. Madzo, T. Skorski, J. Huang

Administrative, technical, or material support (i.e., reporting or organizing

Data, constructing databases): H. Li, Z. Lian, G. Morton, Z. Feng, W. Childers, T. Skorski, J. Huang

Study supervision: T. Skorski, J. Huang

Acknowledgments

We sincerely thank Dr. Peter S. Klein at University of Pennsylvania, Dr. Zhenkun Lou at Mayo Clinic, and Drs. Jean-Pierre Issa and Jaroslav Jelinek at Coriell Institute for Medical Research for their insightful comments and discussion. We thank all the members of Skoriski lab and Huang lab for their help and discussions. We specially thank Steven Schneible at Coriell Institute for assistance with manuscript editing.

Grant Support

J. Huang has been awarded a R01 grant from the NCI (1R01CA255221-01) and a seed grant from Coriell Institute for Medical Research. T. Skorski has been awarded a R01 from NCI (1R01CA244044, 1R01CA247707, 2R01CA186238, 1R01CA237286). The costs of publication of this article were defrayed in part by the payment of page charges. This article must therefore be hereby marked advertisement in accordance with 18 U.S.C. Section 1734 solely to indicate this fact.

References

1. Barkauskaite E, Jankevicius G, Ahel I. Structures and Mechanisms of Enzymes Employed in the Synthesis and Degradation of PARP-Dependent Protein ADP-Ribosylation. Mol Cell **2015**;58:935-46
2. Harrision D, Gravells P, Thompson R, Bryant HE. Poly(ADP-Ribose) Glycohydrolase (PARG) vs. Poly(ADP-Ribose) Polymerase (PARP) - Function in Genome Maintenance and Relevance of Inhibitors for Anti-cancer Therapy. Front Mol Biosci **2020**;7:191
3. Rose M, Burgess JT, O'Byrne K, Richard DJ, Bolderson E. PARP Inhibitors: Clinical Relevance, Mechanisms of Action and Tumor Resistance. Front Cell Dev Biol **2020**;8:564601
4. Gibson BA, Kraus WL. New insights into the molecular and cellular functions of poly(ADP-ribose) and PARPs. Nat Rev Mol Cell Biol **2012**;13:411-24
5. Kim MY, Zhang T, Kraus WL. Poly(ADP-ribosyl)ation by PARP-1: 'PAR-laying' NAD+ into a nuclear signal. Genes Dev **2005**;19:1951-67
6. Huang D, Kraus WL. The expanding universe of PARP1-mediated molecular and therapeutic mechanisms. Mol Cell **2022**;82:2315-34
7. Lord CJ, Ashworth A. Mechanisms of resistance to therapies targeting BRCA-mutant cancers. Nat Med **2013**;19:1381-8

8. Hou P, Wu C, Wang Y, Qi R, Bhavanasi D, Zuo Z*, et al.* A Genome-Wide CRISPR Screen Identifies Genes Critical for Resistance to FLT3 Inhibitor AC220. Cancer Res **2017**;77:4402-13
9. Maifrede S, Le BV, Nieborowska-Skorska M, Golovine K, Sullivan-Reed K, Dunuwille WMB*, et al.* TET2 and DNMT3A Mutations Exert Divergent Effects on DNA Repair and Sensitivity of Leukemia Cells to PARP Inhibitors. Cancer Res **2021**;81:5089-101
10. Hajji N, Garcia-Revilla J, Soto MS, Perryman R, Symington J, Quarles CC*, et al.* Arginine deprivation alters microglial polarity and synergizes with radiation to eradicate non-arginine-auxotrophic glioblastoma tumors. J Clin Invest **2022**;132
11. Barrett T, Suzek TO, Troup DB, Wilhite SE, Ngau WC, Ledoux P*, et al.* NCBI GEO: mining millions of expression profiles--database and tools. Nucleic Acids Res **2005**;33:D562-6
12. Gajan A, Sarma A, Kim S, Gurdziel K, Wu GS, Shekhar MP. Analysis of Adaptive Olaparib Resistance Effects on Cisplatin Sensitivity in Triple Negative Breast Cancer Cells. Front Oncol **2021**;11:694793
13. Elstrodt F, Hollestelle A, Nagel JH, Gorin M, Wasielewski M, van den Ouweland A*, et al.* BRCA1 mutation analysis of 41 human breast cancer cell lines reveals three new deleterious mutants. Cancer Res **2006**;66:41-5
14. Shalem O, Sanjana NE, Hartenian E, Shi X, Scott DA, Mikkelson T*, et al.* Genome-scale CRISPR-Cas9 knockout screening in human cells. Science **2014**;343:84-7
15. Gyorffy B. Survival analysis across the entire transcriptome identifies biomarkers with the highest prognostic power in breast cancer. Comput Struct Biotechnol J **2021**;19:4101-9
16. Dilruba S, Kalayda GV. Platinum-based drugs: past, present and future. Cancer Chemother Pharmacol **2016**;77:1103-24
17. Li H, Liu ZY, Wu N, Chen YC, Cheng Q, Wang J. PARP inhibitor resistance: the underlying mechanisms and clinical implications. Mol Cancer **2020**;19:107
18. McMullen M, Karakasis K, Madariaga A, Oza AM. Overcoming Platinum and PARP-Inhibitor Resistance in Ovarian Cancer. Cancers (Basel) **2020**;12
19. Zhou J, Gelot C, Pantelidou C, Li A, Yucel H, Davis RE*, et al.* A first-in-class Polymerase Theta Inhibitor selectively targets Homologous-Recombination-Deficient Tumors. Nat Cancer **2021**;2:598-610
20. Zatreanu D, Robinson HMR, Alkhatib O, Boursier M, Finch H, Geo L*, et al.* Poltheta inhibitors elicit BRCA-gene synthetic lethality and target PARP inhibitor resistance. Nat Commun **2021**;12:3636
21. Sartori AA, Lukas C, Coates J, Mistrik M, Fu S, Bartek J*, et al.* Human CtIP promotes DNA end resection. Nature **2007**;450:509-14
22. Dias MP, Moser SC, Ganesan S, Jonkers J. Understanding and overcoming resistance to PARP inhibitors in cancer therapy. Nat Rev Clin Oncol **2021**;18:773-91
23. Vilas CK, Emery LE, Denchi EL, Miller KM. Caught with One's Zinc Fingers in the Genome Integrity Cookie Jar. Trends Genet **2018**;34:313-25
24. Singh JK, Smith R, Rother MB, de Groot AJL, Wiegant WW, Vreeken K*, et al.* Zinc finger protein ZNF384 is an adaptor of Ku to DNA during classical non-homologous end-joining. Nat Commun **2021**;12:6560

25. Moison C, Chagraoui J, Caron MC, Gagne JP, Coulombe Y, Poirier GG*, et al.* Zinc finger protein E4F1 cooperates with PARP-1 and BRG1 to promote DNA double-strand break repair. Proc Natl Acad Sci U S A **2021**;118
26. Nowsheen S, Aziz K, Luo K, Deng M, Qin B, Yuan J*, et al.* ZNF506-dependent positive feedback loop regulates H2AX signaling after DNA damage. Nat Commun **2018**;9:2736
27. Moquin DM, Genois MM, Zhang JM, Ouyang J, Yadav T, Buisson R*, et al.* Localized protein biotinylation at DNA damage sites identifies ZPET, a repressor of homologous recombination. Genes Dev **2019**;33:75-89

Figure legends:

Figure 1. A CRISPR screen in MDA-MB-436 *BRCA1*-mutated breast cancer cells uncovered *ZNF251* genes whose loss-of-function confers olaparib resistance. A. A simplified schematic of the olaparib resistance CRISPR screen with MDA-MB-436 breast cancer cells. B, C. Enrichment of specific sgRNAs that target each gene after 14 days of olaparib treatment and identification of top candidate genes. The x axis represents enriched genes, and the y axis represents sgRNA enrichment score, which was calculated using (sgRNA number from the reads)/(sgRNA number in the library)/$\log_2$ (average abundance). Arrow indicates *ZNF251* gene. D. Top panel: T7EN1 assay analysis of specific sgRNA-mediated in/dels at *ZNF251* locus in MDA-MB-436 cells. Bottom panel: Cell growth curve of parental (*ZNF251* WT) and *ZNF251* KO MDA-MB-436 breast cancer cells following treatment with olaparib. The results represent three independent experiments. E. Top panel: Sanger sequencing data of three *ZNF251* KO clones. Bottom panel: Cell growth curve of WT and three *ZNF251* KO single clone breast cancer cells following treatment with olaparib. The results represent three independent experiments. F. *ZNF251* KO was constructed in HCC1937 (*BRCA1*+ or *BRCA1*-) lines and the resistance to olaparib was measured. The results represent three independent experiments. G, H. The effect of olaparib on the growth of wildtype and *ZNF251* KO MDA-MB-436 breast cancer cells xenografts in immune-deficient NOD/SCID/IL-2Rγ (NSG) mice was tested. The results represent three independent experiments.

Figure 2. *ZNF251 KO* caused resistance to multiple PARPis in different breast and ovarian cancer lines. A, B. *ZNF251* KO was constructed in MDA-MB-436 and Ovcar8 cell lines and the resistance to olaparib, niraparib, veliparib, NMS-P118, stenoparib was measured compared to wildtype (WT) control. The results represent three independent experiments.

Figure 3. *ZNF251* KO led to resistance to the platinum-based drugs. A-C, the resistance of WT and *ZNF251* KOs to cisplatin, carboplatin, 5-fluorouracil was tested. The results represent three independent experiments.

Figure 4. *ZNF251* KO cells show resistance to DNA polymerase θ inhibitors. Sensitivity of MDA-MB-436 WT and MDA-MB-436 *ZNF251* KO cells to DNA polymerase θ inhibitors A. ART-812 and B. ART-558 at indicated concentrations. The results represent mean % colonies ± SDs when compared to untreated cells.

Figure 5. *ZNF251* KO led to upregulated HR and NHEJ repair under treatment of olaparib. A. Comet assay was performed to examine whether *ZNF251* KO affects the amount of DSBs in MDA-MB-436 cells. B. Reporter assay was carried out to determine the change of DSB repair pathways in MDA-MB-436 and Ovcar8 cells. C. Representative western blots to examine the expression of key components of DSB repair, including HR, D-NHEJ, and Alt-NHEJ.

Figure 6. Blockade of D-NHEJ pathway reversed PARPi resistance of *ZNF251* KO *in vitro* and *in vivo*. A. wildtype (WT) and *ZNF251* KO MDA-MB-436 cells were treated with olaparib and RAD51 inhibitor B02 (4 μM). B. wildtype (WT) and *ZNF251* KO MDA-MB-436 cells were treated with olaparib and DNA-PKcs inhibitor PIK-75 (8 nM). C. Schematic description of our in *vivo* experimental design. D, E. The effect of olaparib and olaparib+PIK-75 on the growth of *ZNF251* wildtype and *ZNF251* KO MDA-MB-436 breast cancer cells xenografts in NSG mice was tested. Results represent mean tumor volume and weight ± SDs.

Supplementary Fig. 1. The dose response of MDA-MB-436 breast cancer cells to olaparib. A. the growth curve of MDA-MB-436 breast cancer cells treated with DMSO or various doses of olaparib. B. The growth curve of MDA-MB-436 breast cancer cells treated with various doses of olaparib.

Supplementary Fig. 2. Transfection of wild type *ZNF251* on a plasmid reversed olaparib resistance of *ZNF251* KO breast cancer cells. Wildtype (WT), WT cells transfected with PC DNA3.1 vector, *ZNF251* KO and *ZNF251* KO transfected with *ZNF251* cDNA on PC DNA3.1 were treated with olaparib for 72 hours and cell viability was measured.

Supplementary Fig. 3. *ZNF251* KO doesn't affect cell growth in the absence of PARPi treatment. A. Cell growth of WT, *ZNF251* KO1, *ZNF251* KO2 and *ZNF251* KO3 MDA-MB-436

breast cancer cells was measured. B. Cell growth of WT, *ZNF251* KO1, *ZNF251* KO2 and *ZNF251* KO3 Ovcar8 ovarian cancer cells was measured.

Supplementary Fig. 4. Bioinformatic analysis showed that ZNF251 expression is corelated with PARPi and platinum drugs sensitivity as well as prognosis of breast cancer patients. A. *ZNF251* expression was correlated with olaparib resistance of breast cancer cells. Box-whisker plots indicating the *ZNF251* expression values of olaparib sensitive and resistant cells collected from the Gene Expression Omnibus (GEO) database datasets. Green color plot represents sensitivity towards PARPi whereas red color plot represents resistance towards PARPi. Box-whisker plot for olaparib sensitive and resistant cells was generated using the GEO dataset GSE165914. Y-axis represents the expression of *ZNF251* in the respective cells. Statistical analysis was performed using the 2-tailed Student's t test. *p-value<0.05. B-D. *ZNF251* expression is positively correlated with sensitivity to olaparib, cisplatin and carboplatin of the breast cancer cells by CellMiner database analysis. E. Low *ZNF251* expression is correlated with worse survival for breast cancer patients using online Kaplan-Meier plotter (https://kmplot.com/analysis/index.php?p=service&cancer=breast), which integrates gene expression and clinical data from 2,032 patients.

Supplementary Fig. 5. Quantification of western analysis of vehicle-treated or olaparib-treated wildtype (WT) and *ZNF251* KO breast cancer cells. A-D. Densitometry was measured for western analysis of key factors involved in DDR, HR, D-NHEJ, alt-NHEJ pathways.

Supplementary Fig. 6. Treating *ZNF251* KO breast cancer cells with Rad51 inhibitor B02 at 16μM cannot reverse olaparib resistance. Wildtype (WT) and *ZNF251* KO breast cancer cells were treated with vehicle, or olaparib, or B02(16μM) or olaparib+B02(16μM) for 72 hours and the cell viability was measured.

Figure 1. A genome-wide CRISPR screen identified *ZNF251* whose loss-of-function caused Olaparib resistance in a breast cancer line

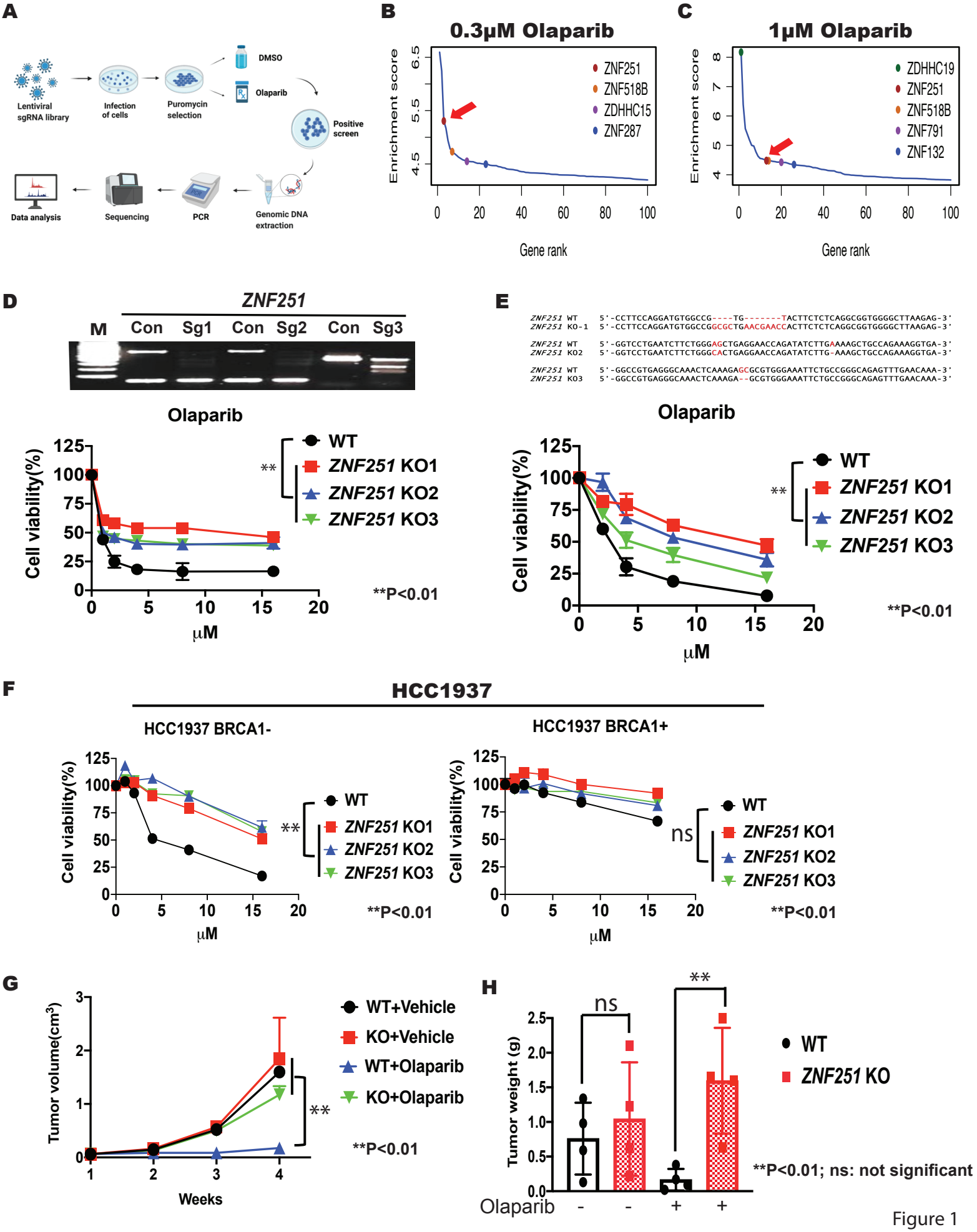

Figure 1

Figure 2. *ZNF251* KO caused resistance to multiple PARP inhibitors in different cancer lines

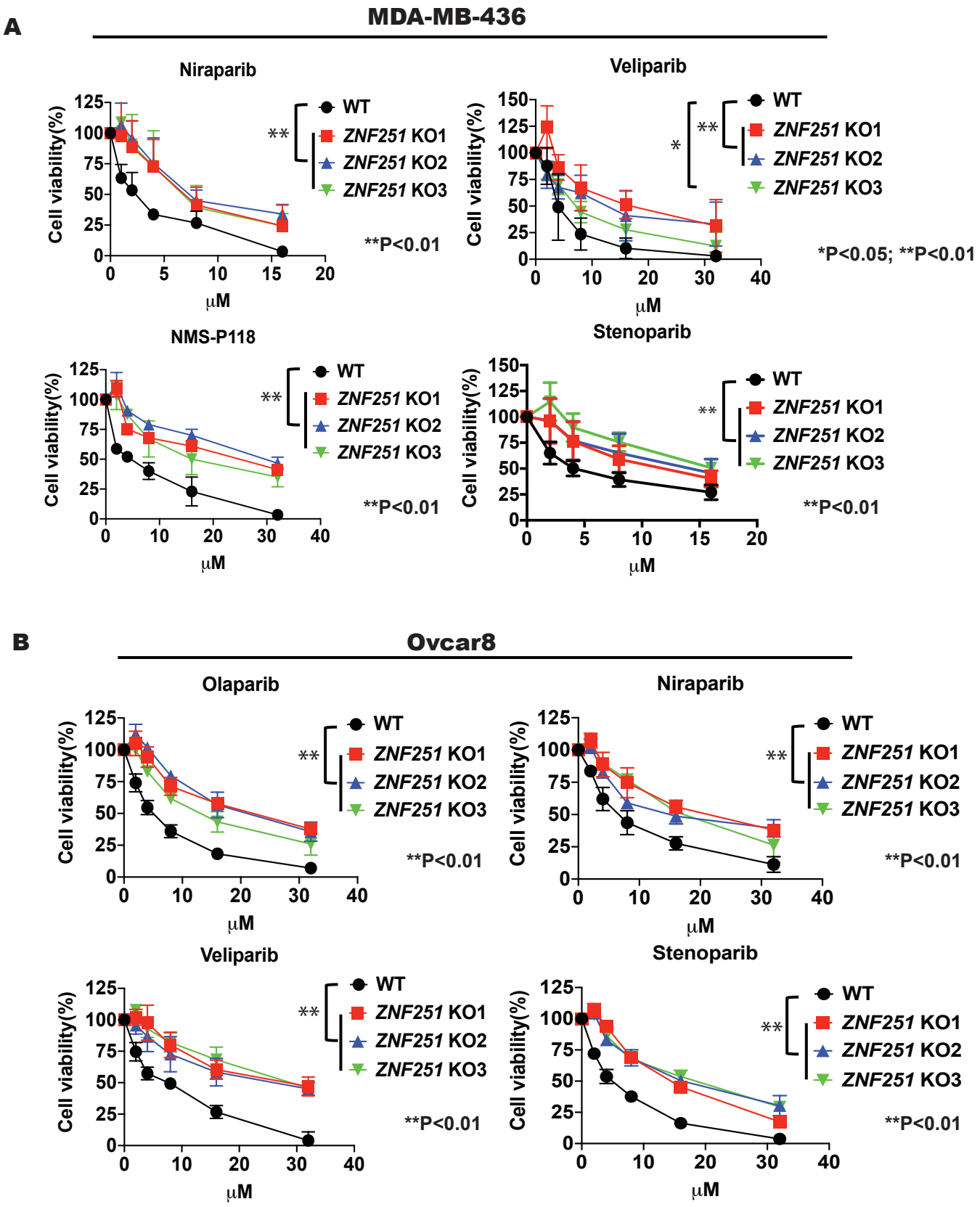

Figure 3. ***ZNF251*** **KO led to resistance to the platinum-based drugs**

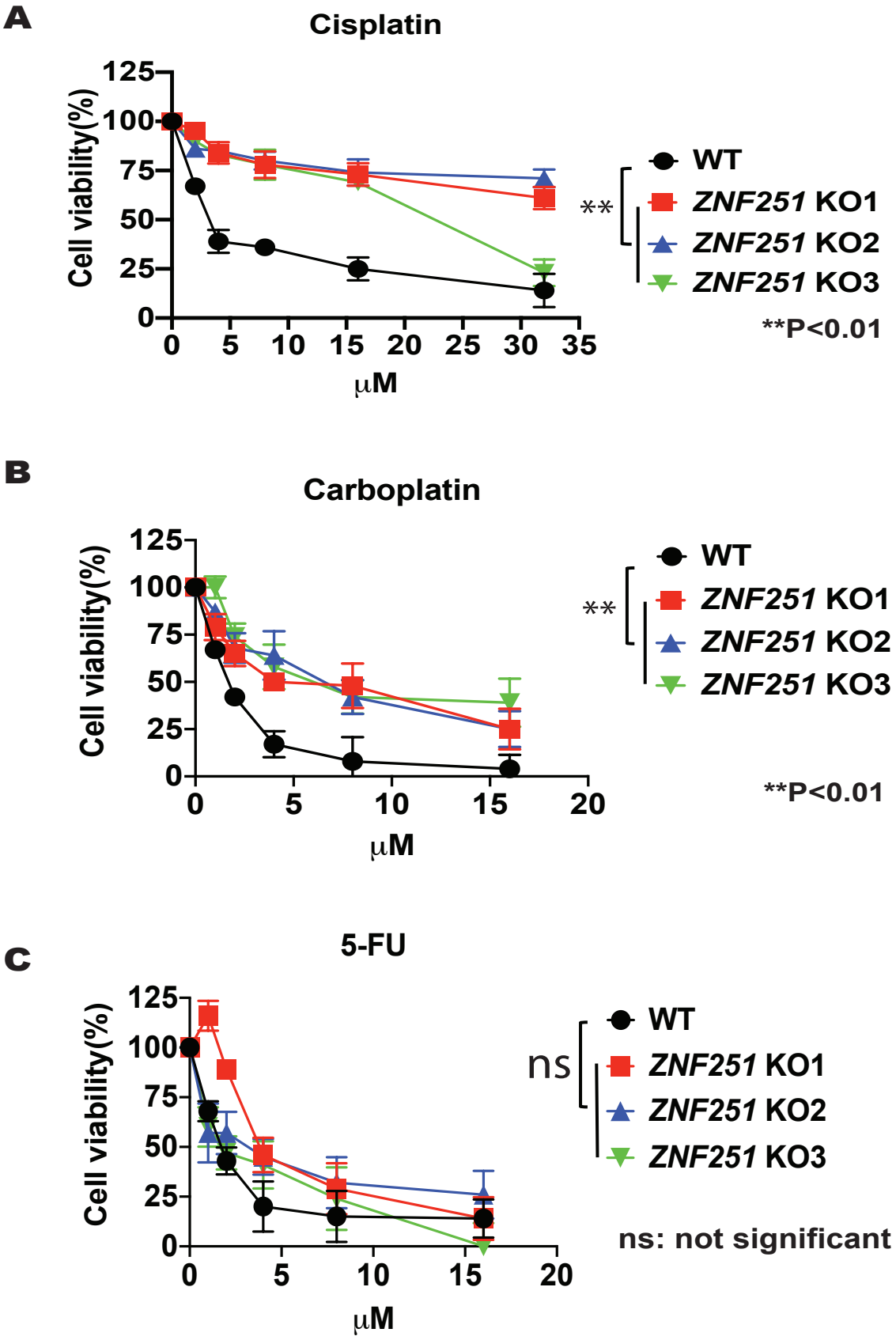

Figure 4. ***ZNF251*** **KO cells showed resistance to Polymeraseϑ inhibitors**

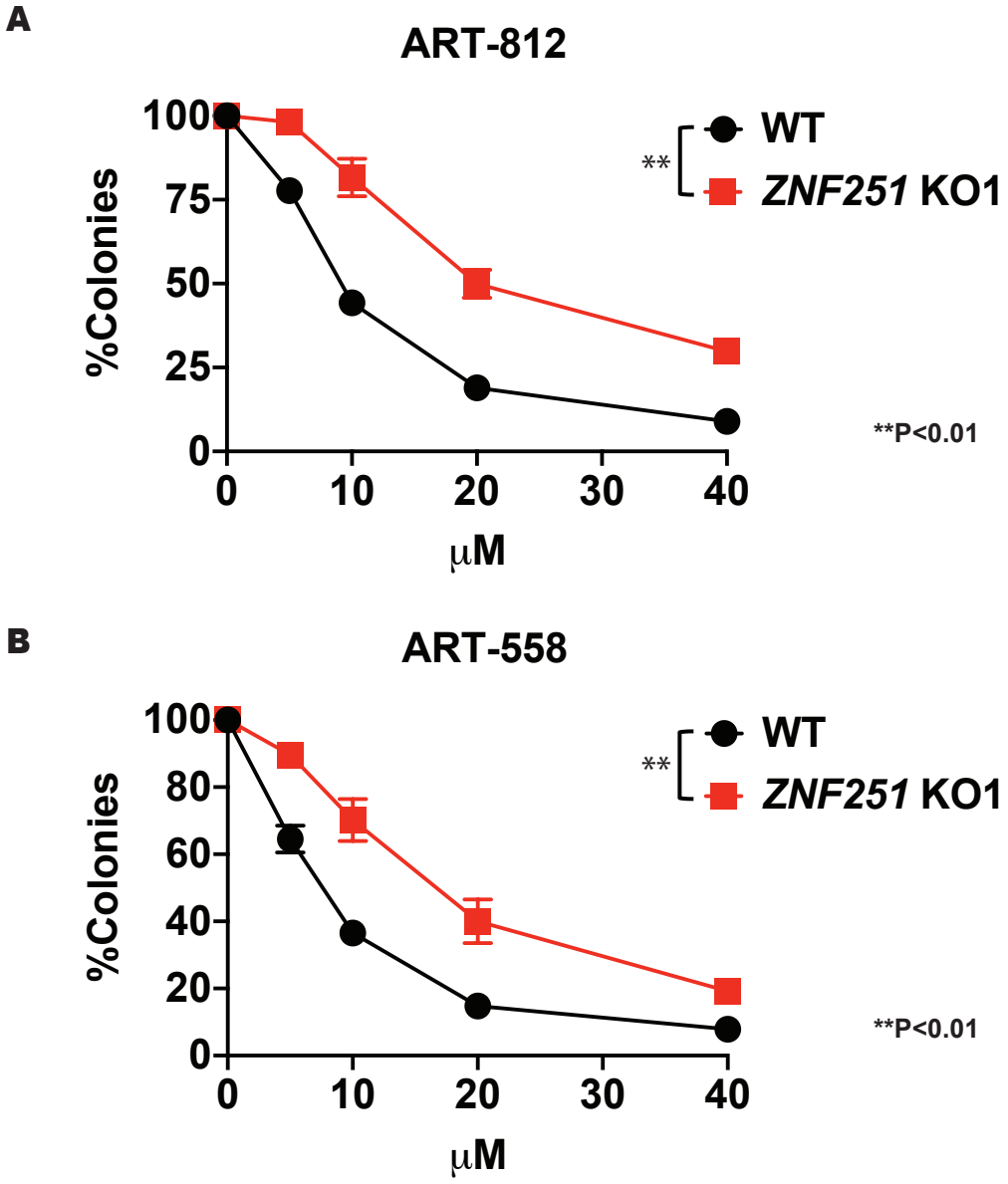

Figure 5. ***ZNF251*** **KO led to upregulated HR and NHEJ repair with treatment of Olaparib**

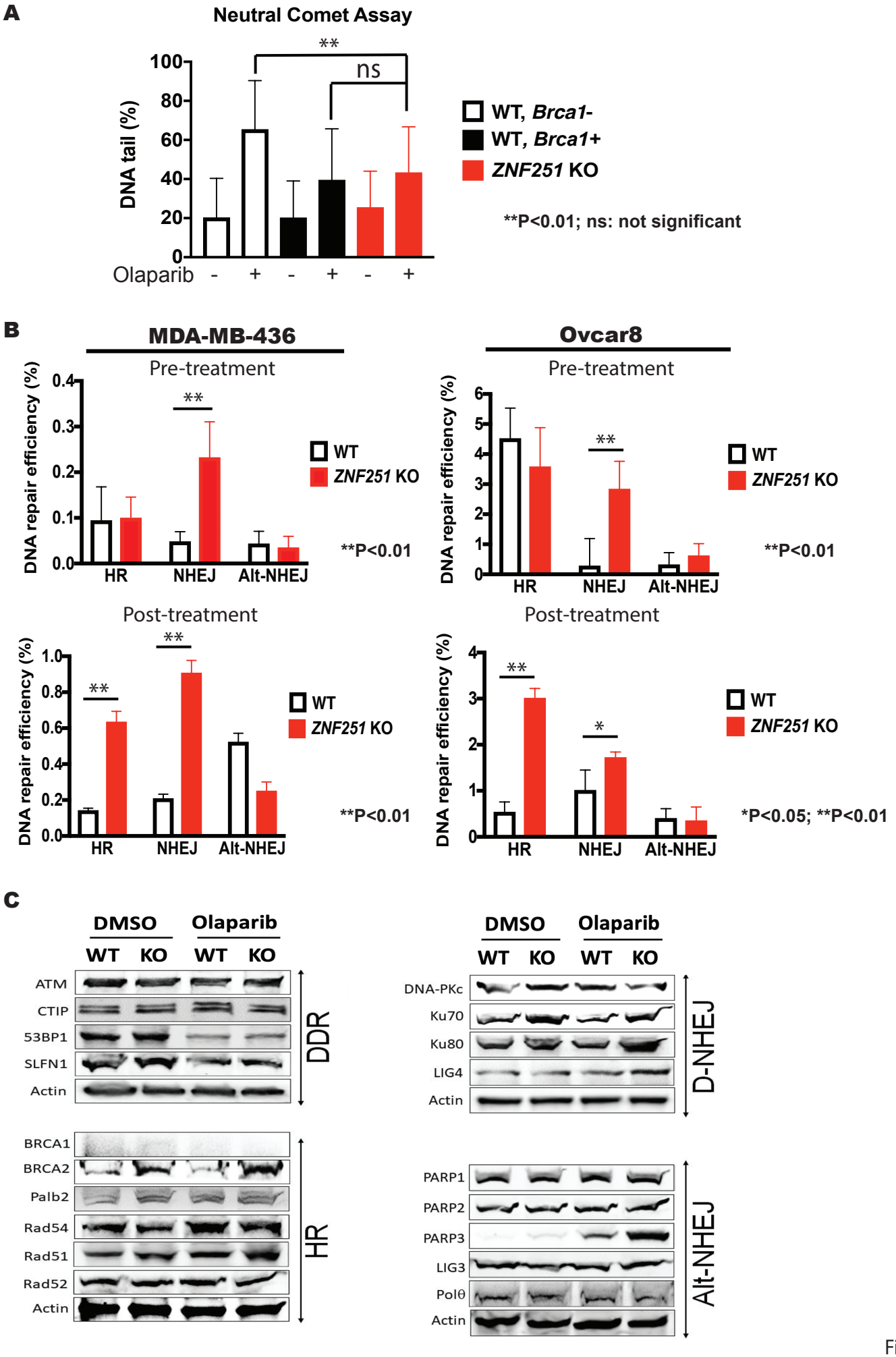

Figure 5
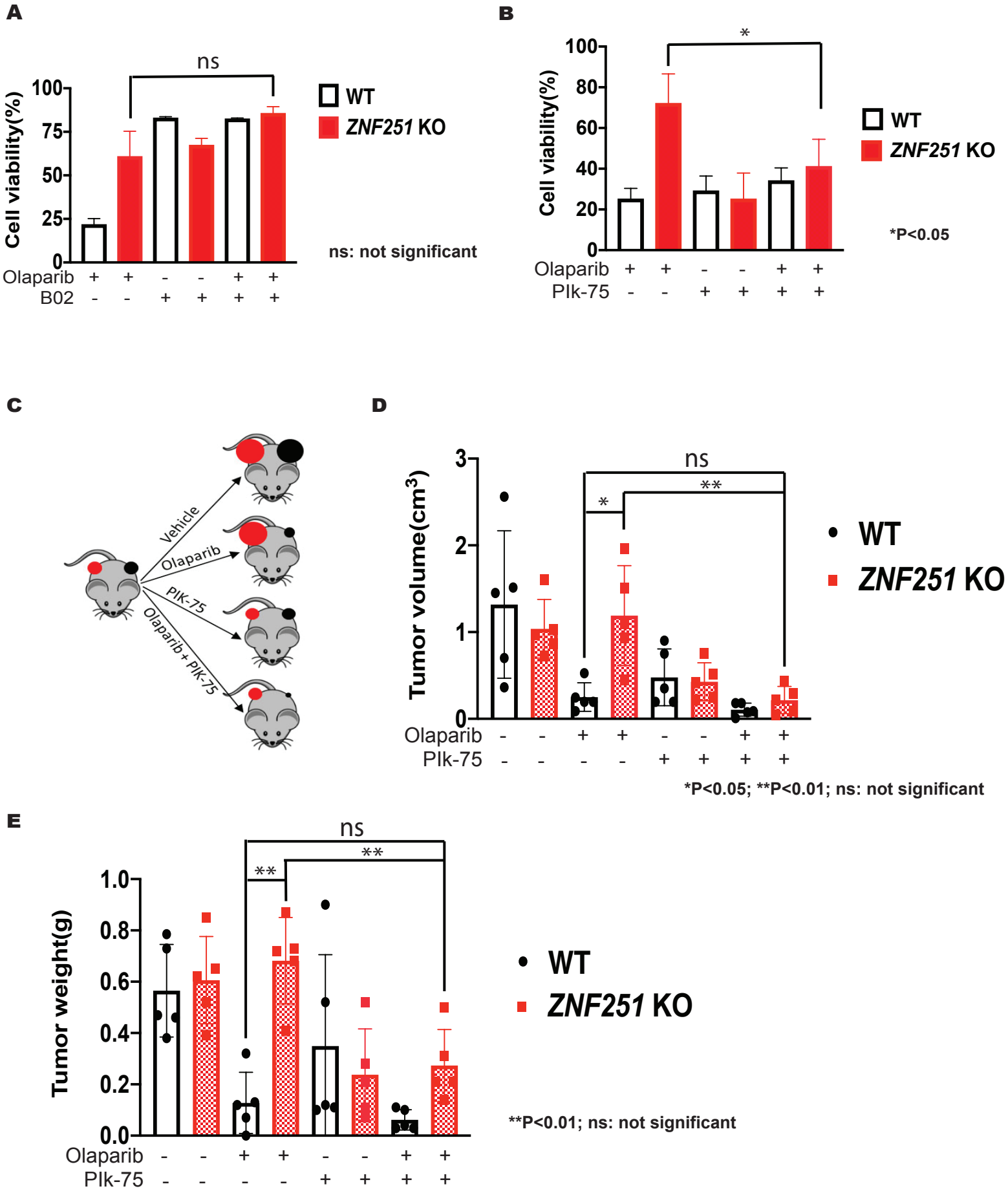
Figure 6. Inhibition of D-NHEJ pathway reversed PARPi resistance in BRCA1-mutated *ZNF251* KO cells